Biogeosciences

Open Access

EGU

Research article

Ocean alkalinity enhancement approaches and the predictability of runaway precipitation processes: results of an experimental study to determine critical alkalinity ranges for safe and sustainable application scenarios

Niels Suitner[1], Giulia Faucher[2], Carl Lim[3], Julieta Schneider[2], Charly A. Moras[4], Ulf Riebesell[2], and Jens Hartmann[1]

[1]Institute for Geology, Universität Hamburg, Bundesstrasse 55, 20146 Hamburg, Germany
[2]GEOMAR Helmholtz Centre for Ocean Research Kiel, Wischhofstrasse 1–3, 24148 Kiel, Germany
[3]KU Leuven, Department of Materials Engineering, 8200 Bruges, Belgium
[4]Faculty of Science and Engineering, Southern Cross University, Lismore, NSW 2480, Australia

Correspondence: Niels Suitner (niels.suitner@uni-hamburg.de) and Jens Hartmann (geo@hattes.de)

Abstract. To ensure the safe and efficient application of ocean alkalinity enhancement (OAE), it is crucial to investigate its impacts on the carbonate system. While modeling studies reported a sequestration potential of 3–30 Gt carbon dioxide (CO_2) per year (Oschlies et al., 2023), there has been a lack of empirical data to support the applicability of this technology in natural environments. Recent studies have described the effect of runaway carbonate precipitation in the context of OAE, showing that calcium carbonate ($CaCO_3$) formation was triggered if certain $\Omega_{aragonite}$ saturation thresholds were exceeded. This effect could potentially lead to a net loss of the initially added alkalinity, counteracting the whole concept of OAE. The related precipitation can adversely affect the carbon storage capacity and may in some cases result in CO_2 emissions. Experiments at the Espeland marine biological station (Bergen, Norway) were conducted to systematically study the chemical consequences of OAE deployment. The experiments lasted for 20–25 d to monitor the temporal development of carbonate chemistry parameters after alkalinity addition and the subsequent triggered carbonate precipitation process. Identified uniform patterns before and during the triggered runaway process can be described by empirical functional relationships. For approaches equilibrated to the CO_2 concentration of the atmosphere, total alkalinity (TA) levels of up to $6500\,\mu mol\,kg^{-1}$ remained stable without loss of total alkalinity (TA) for up to 20 d. Higher implemented TA levels, up to $11\,200\,\mu mol\,kg^{-1}$, triggered runaway carbonate formation. Once triggered, the loss of alkalinity continued until the $\Omega_{aragonite}$ values leveled out at 5.8–6.0, still resulting in a net gain of $3600–4850\,\mu mol\,kg^{-1}$ in TA. The non-CO_2-equilibrated approaches, however, only remained stable for TA additions of up to $1000\,\mu mol\,kg^{-1}$. The systematic behavior of treatments exceeding this level allows us to predict the duration of transient stability and the quantity of TA loss after this period. Once triggered, the TA loss continued in the non-CO_2-equilibrated approaches until $\Omega_{aragonite}$ values of 2.5–5.0 were reached, in this case resulting in a net loss of TA. To prevent a net loss of TA, treated water must be diluted below the time-dependent critical levels of TA and $\Omega_{aragonite}$ within the identified transient stability duration. Identified stability and loss patterns of added TA depend on local environmental conditions impacting the carbonate system, such as salinity, temperature, biological activity, and particle abundance. Incorporating such stability and loss patterns into ocean biogeochemical models, which are capable of resolving dilution processes of treated and untreated water parcels, would, from a geochemical perspective, facilitate the prediction of safe local application levels of OAE. This approach would also allow an accurate determination of the fate of added alkalinity and a more realistic carbon storage potential estimation compared to the assessments that neglect carbonate system responses to OAE.

1 Introduction

At the current greenhouse gas emission rates, global warming well below 2 °C compared to pre-industrial levels, as targeted by the Paris Agreement (UNFCCC, 2015), might not be achievable (Meinshausen et al., 2009; Rogelj et al., 2016). To prevent such a development, international efforts have turned the spotlight on reducing greenhouse gas emissions globally. However, to comply with the climate goals, greater attention needs to be paid to carbon dioxide removal (CDR) technologies. One such marine-based technology is ocean alkalinity enhancement (OAE), a strategy that aims to chemically sequester carbon dioxide (CO_2) as carbonate (CO_3^{2-}) or bicarbonate (HCO_3^-) ions in ocean water (Kheshgi, 1995; NASEM, 2022). The concept of OAE strives to increase the inorganic carbon storage capacity by increasing the total alkalinity (TA) of seawater (Caldeira and Rau, 2000; Hartmann et al., 2013; Köhler et al., 2010; Schuiling and Krijgsman, 2006). Naturally, inorganic carbon is stored in the ocean over periods of time ranging from 10 000 to 100 000 years (Berner et al., 1983; Mackenzie and Garrels, 1966). This long-term carbon storage potential makes OAE a preferred option over other suggested marine CDR methods. An accompanying benefit of this strategy is the parallel increase in pH, thus counteracting ocean acidification (Ilyina et al., 2013; Köhler et al., 2010).

Tests for OAE under close-to-natural conditions are still scarce (Albright et al., 2016; Cyronak et al., 2023; Ferderer et al., 2022; Paul et al., 2023; Sánchez et al., 2023; Yang et al., 2023). For a safe and efficient application of OAE, it is crucial to assess the induced changes in carbonate chemistry and investigate their potential environmental impacts (Bach et al., 2019; Riebesell et al., 2023).

In isolated case studies, prototypes for alkalinity enhancement have already been put into practice to counteract lake acidification (e.g., Koch and Mazur, 2016; Benthaus et al., 2020) or were discussed in the context of river water alkalinity enhancement (Sterling et al., 2023). Various application methods for OAE have been proposed, ranging from spreading ground rock powder or mineral phases (Kheshgi, 1995) to liquid addition of alkaline solutions directly into the seawater or via rivers (Hartmann et al., 2013; Sterling et al., 2023) and electrochemical alkalinity generation (Eisaman et al., 2023; Renforth and Henderson, 2017). Alkalinity enhancement could be achieved in a CO_2-equilibrated or non-CO_2-equilibrated manner, as discussed in Schulz et al. (2023). In the non-equilibrated scenario, the seawater would gradually equilibrate over time by absorbing atmospheric CO_2. The CO_2-equilibrated approach consists of adding alkalized water that is already in equilibrium with the atmosphere. This means that, at the point of addition, the water is put into equilibrium with the atmosphere either with technological apparatus before release or with a CO_2 source being used to bring the water into equilibrium after TA addition. Alternatively, solids like Na_2CO_3 or $NaHCO_3$ could be used

for OAE, since they are already used to capture CO_2 from a source (e.g., Forster 2012, 2014) before the alkaline products are disposed of.

To illustrate the impact of different alkalinity addition scenarios on various carbonate chemistry parameters, Fig. 1 presents a TA : DIC diagram modeled after Deffeyes (1965). Besides dissolved inorganic carbon (DIC) and total alkalinity, the Deffeyes diagram provides information on the corresponding pH, pCO_2, and saturation state for aragonite ($\Omega_{aragonite}$).

Surpassing critical thresholds of $\Omega_{aragonite}$ saturation states for a certain period of time could result in calcium carbonate ($CaCO_3$) precipitation (Schulz et al., 2023; Zeebe and Wolf-Gladrow, 2001). This phenomenon could lead to a runaway process, as observed in laboratory-based experimental studies conducted by Moras et al. (2022), Hartmann et al. (2023), Fuhr et al. (2022), and Pan et al. (2021). This process could lead to a net loss in CO_2 storage potential and result in a leakage of TA and DIC.

Considering the complexity and variety of possible environmental impacts of OAE scenarios, systematic empirical investigations of alkalinization approaches seem to be vital in providing meaningful sustainability assessments. This study aims to assess the geochemical impacts of alkalinity addition in seawater by refining and improving upon the experimental setup of Hartmann et al. (2023), testing CO_2-equilibrated and non-equilibrated TA enhancement scenarios in natural seawater. Incubation experiments were conducted with extended TA ranges and run times, along with increased sampling frequency and enhanced resolution of the TA gradients. Experiments were designed to identify stability ranges of the added alkalinity and characterize critical thresholds that trigger the runaway precipitation process.

2 Methods

2.1 Experimental setup

Four sets of experiments were conducted between May and July 2022 using natural seawater from Raunefjorden (60.27° N, 5.20° E), close to the Espeland marine biological station (Bergen, Norway). All four experiments used the same setup. Firstly, 250 mL polystyrene cell culture bottles were filled with filtered seawater in a flow-through incubation box (PMMA) and incubated outdoors to follow the local light conditions (see Fig. S1 in the Supplement). The box was covered in blue foil (172 Lagoon Blue Foil, LEE Filters, Burbank, CA, United States) to mimic the light conditions in the fjord at a depth of ∼ 5 m. The temperature was regulated by recirculating fjord water in the incubation box, thus ensuring that the incubation temperature matched that of the fjord. To prevent the occurrence of substantial headspace throughout the experiment, each treatment level was divided into three to four separate bottles. The divi-
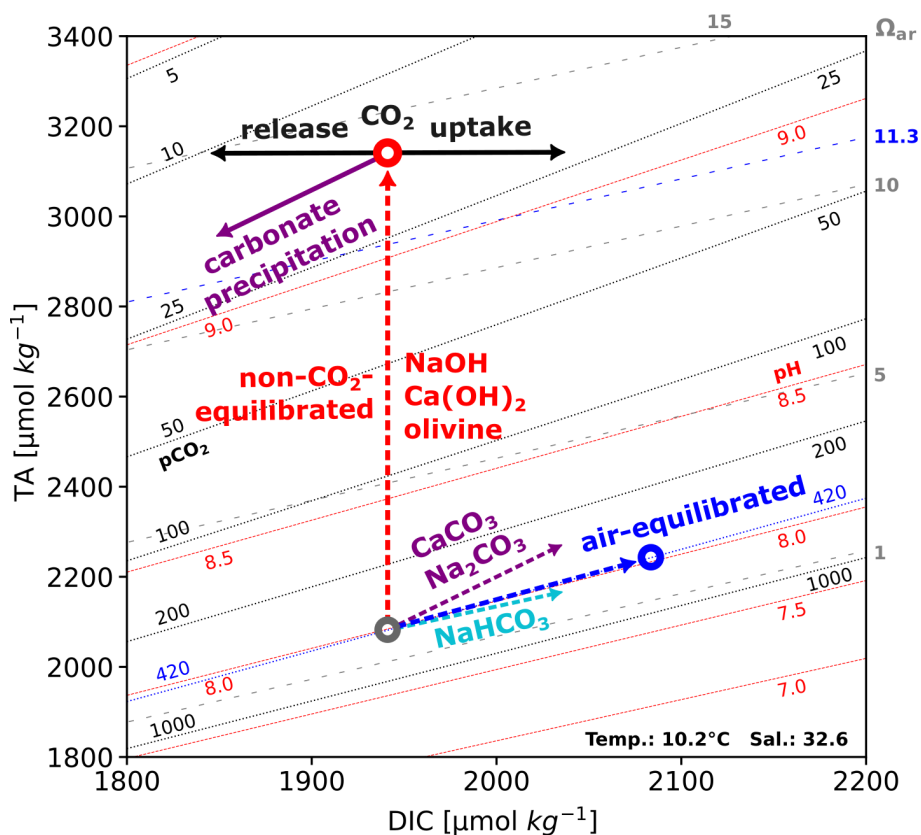
Figure 1. Example of a TA : DIC diagram after Deffeyes, 1965, in the context of OAE. Background contours represent isolines of pH (red), $\Omega_{aragonite}$ (dotted gray), and pCO_2 (black) values, and shown contours reflect pH, pCO_2, and $\Omega_{aragonite}$ values for varying TA and DIC levels at given temperature and salinity conditions. Dashed arrows show the impact of indicated alkalinization approaches; e.g., a non-CO_2-equilibrated TA addition could be realized by injection or dissolution of sodium hydroxide (NaOH), and an air-equilibrated TA addition (in equilibrium with the atmosphere; pCO_2 420 µatm) could be achieved by utilizing a combination of $NaHCO_3$ and Na_2CO_3. During non-CO_2-equilibrated approaches, the pCO_2 of the manipulated water is reduced, creating the potential of CO_2 uptake (black arrow) from the atmosphere; if the TA addition surpasses certain critical ranges (for surface-free waters under the given conditions here indicated by the blue $\Omega_{aragonite}$ contour of 11.3, calculated after Marion et al., 2009), carbonate precipitation (purple arrow) results in the reverse changes in $CaCO_3$ dissolution.

Table 1. Overview experimental design (Bergen 2022).

No.	Seawater conditions	CO_2 state to atmosphere	Alkaline material	Run time (days)	Range TA_{added} ($\mu mol\,kg^{-1}$)	TA_{added} gradient steps ($\mu mol\,kg^{-1}$)	Temperature (°C)
I	Biotic	Air-equilibrated	$Na_2CO_3/NaHCO_3$	20	0–2800	200	12–15
	Abiotic			20	0–9200	200/800	12–16
II	Biotic	Non-equilibrated	NaOH	25	0–2800	200	10–11
	Abiotic			25	0–3400	200	11–13

sion allowed progressive volume removal during sampling while reducing the potential for gas exchange processes. Within each experiment, a new set of bottles was opened sequentially after three to four samplings. Alkalinity was enhanced using a 0.5 M NaOH (sodium hydroxide) stock solution for the non-CO_2-equilibrated treatments and a combination of $NaHCO_3$ (sodium bicarbonate, 0.4 M) and Na_2CO_3

(sodium carbonate, 0.2 M) stock solutions for the preparation of the CO_2-equilibrated treatments. The latter were adjusted to attain equilibrium with the surrounding air's CO_2 concentration ($\sim$ 420 µatm). For each of the two, the experimental setups encompassed (1) abiotic conditions, achieved by removing organisms via filtration through a 0.2 µm filter, and (2) biotic conditions, where only the small phyto-

plankton community was included by using a 50 μm filter mesh to remove larger particles and organisms. The categorization into abiotic and biotic treatments aimed to determine the potential influences of biological activity or naturally occurring sediments, while also preserving the comparability of the experimental setup described in Hartmann et al. (2023). An overview of the TA levels reached and the step sizes, run times, and temperature ranges is given in Table 1. The experiments were conducted over a span of 2 months, with each incubation run for 20 or 25 d. The experiments were therefore partially separated in time, resulting in slight variations in starting conditions and average temperatures, ranging from 10 to 16 °C. Biotic and abiotic treatments were simultaneously conducted within each equilibration mode. The initial carbonate chemistry parameters of the collected seawater before manipulation were relatively constant for all approaches ($TA_{initial} \sim 2190 \pm 10\,\mu mol\,kg^{-1}$, DIC $\sim 1890 \pm 20\,\mu mol\,kg^{-1}$, pH $\sim 8.25 \pm 0.05$, and sal. $\sim 32.6 \pm 0.1$).

2.2 Sampling and measurements

For carbonate chemistry analysis, 40–50 mL of incubated water was taken per sampling day and treatment level. Using a peristaltic pump connected to a 0.2 μm syringe filter, samples were filtered immediately to stop further reactions, remove particles, and prepare each sample for measurements. All treatments were measured without replicates for TA, pH, temperature, and salinity, and biotic treatments were further analyzed to assess the biological responses. An accompanying publication will describe the impact of enhanced alkalinity on the included phytoplanktonic communities during the first 6 d of the biotic incubation experiments. A selection of filtrates was saved for scanning electron microscopy (SEM) analysis. Minor shifts in pH, DIC, and $\Omega_{aragonite}$ originate from increasing water temperatures during the run times of the experiments, photosynthetic activity in the biotic approaches, or minor ingassing from the headspace of the reactor bottles (see Table S1 in the Supplement).

Methods and devices for measuring TA, pH, temperature, and salinity were identical to experiments I and II from Hartmann et al. (2023). Total alkalinity was determined by titration with 0.02 M hydrochloric acid, using an 888 Titrando autosampler (Metrohm). TA measurements were corrected against certified reference materials (CRM batch 193), supplied by the Prof. Andrew G. Dickson laboratory, Scripps Institution of Oceanography (USA). A WTW multimeter (MultiLine®Multi 3630 IDS) was used to measure pH (SenTix 940 pH electrode), temperature, and salinity (TetraCon 925 cell, Xylem). The pH probe was calibrated with WTW buffer solutions according to NIST/PTB in four steps (1.679–9.180 at 25 °C) and corrected for seawater after Badocco et al. (2021). DIC, pCO_2, and saturation states were calculated using CO2SYS-Excel version 2.5 (Pierrot et al., 2006), including error propagations based on Orr et al. (2018) (un-

certainties were set to $\pm 5\,\mu mol\,kg^{-1}$ for TA, ± 0.02 for pH, ± 0.1 °C for temperature, and ± 0.1 for salinity). Constants in CO2SYS were set to Lueker et al. (2000) for K_1 and K_2, Dickson (1990) for $KHSO_4$, Perez and Fraga (1987) for KHF, and Lee et al. (2010) for $[B]_T$ value, and the pH was calculated on the total scale.

The physical appearance of precipitated particles and their elemental composition were analyzed by two separate SEM setups: (1) Hitachi tabletop microscope TM4000Plus (University of Hamburg) and (2) ZEISS Gemini Ultra55 Plus (CAU Kiel), both equipped with an energy-dispersive X-ray spectroscopy (EDX) detector.

2.3 ΔTA equation

Based on the concept from Hartmann et al. (2023), the subsequent equation is utilized to simplify the characterization of values reached or alterations in TA:

$$\Delta TA_{net} = TA_{final} - TA_{initial} = \Delta TA_{added} + \Delta TA_{loss},$$

where ΔTA_{net} is the net change in TA, TA_{final} is the absolute reached TA after TA addition (measured), $TA_{initial}$ is the initial TA of used seawater (measured), ΔTA_{added} is the amount of increased TA by alkalinity addition, and ΔTA_{loss} is the amount of TA decline during the experiment (negative sign).

3 Results

3.1 CO_2-equilibrated experiments

In the biotic CO_2-equilibrated experiment, an air-equilibrated alkalinization of up to $2800\,\mu mol\,kg^{-1}$ could be achieved during the 20 d run time. All carbonate chemistry parameters remained constant, showing that a TA addition slightly above the estimated critical $\Omega_{aragonite}$ value for pseudo-homogenous precipitation of 11.3 (after Marion et al., 2009) could be achieved. This level was maintained for 20 d without causing any $CaCO_3$ precipitation, as illustrated in Fig. 2a–c.

By extending the alkalinity range up to $9200\,\mu mol\,kg^{-1}$ in the abiotic air-equilibrated experiment, $\Omega_{aragonite}$ values far above critical levels were reached, resulting in extensive carbonate precipitation in a runaway style (Fig. 2d–f). All targeted alkalinity levels were achieved ~ 3 min after alkalinity addition (day 0), and a decline in TA was observed in treatments above ΔTA 3600 (corresponding to $\Omega_{aragonite}$ of 14.6). Starting with the highest treatment levels after 1 d, precipitation was triggered in all batches with a ΔTA above 3600 over the run time of 20 d (see Fig. 2d). Following precipitation, once $\Omega_{aragonite}$ reached values of 5.8–6.0, the process halted, resulting in a linear alignment of final TA values. The TA loss rate was significantly reduced towards the end of the precipitation procedure; however, it could not be excluded
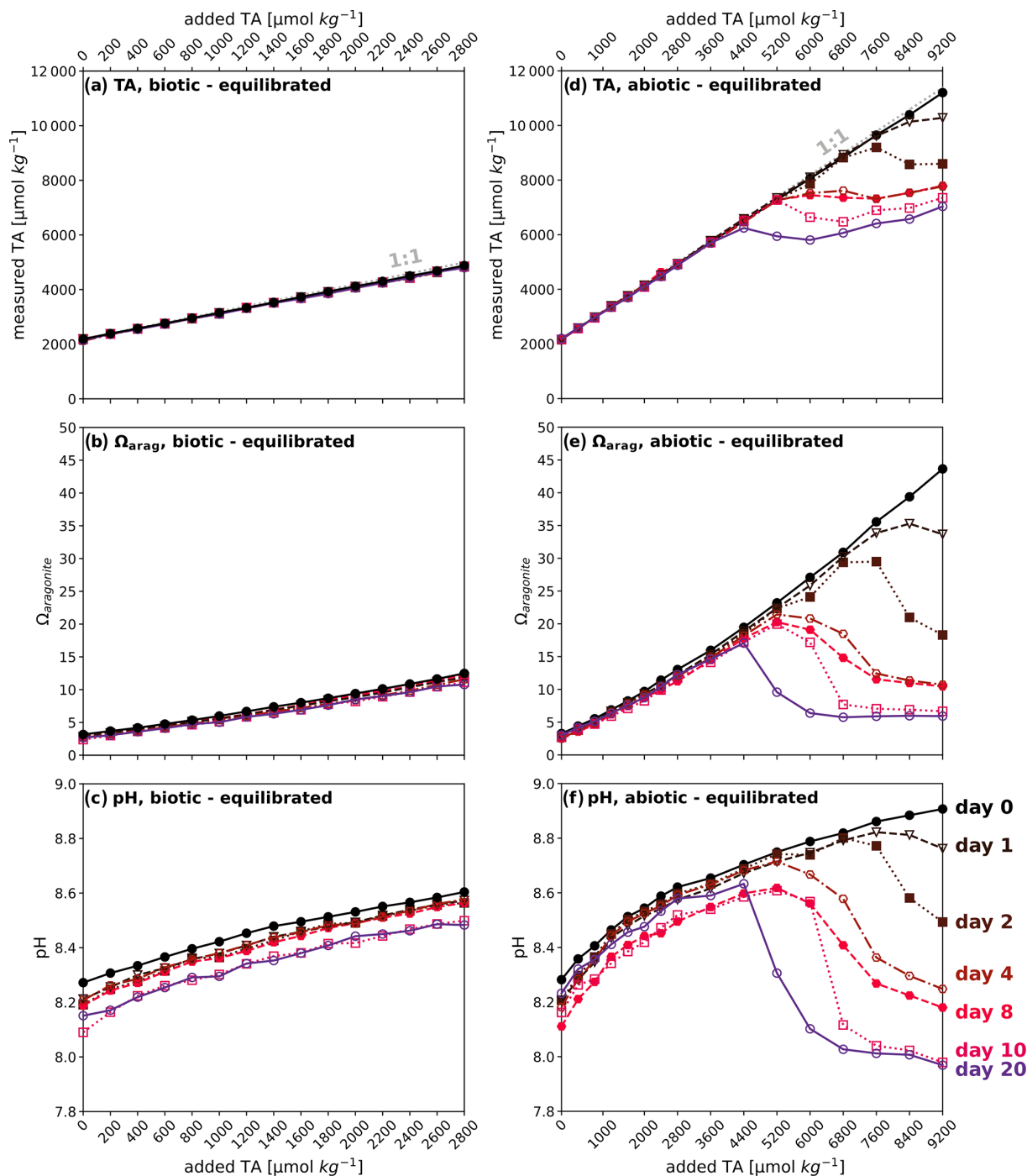
Figure 2. Temporal TA, $\Omega_{aragonite}$, and pH evolution in CO_2-equilibrated experiments, under biotic **(a–c)** and abiotic **(d–f)** conditions. Each diagram represents a specific carbonate chemistry parameter investigated, i.e., measured TA **(a, d)**, $\Omega_{aragonite}$ **(b, e)**, and pH **(c, f)** as a function of added TA and time point. The legend for sampling days is given in panel **(f)**; data points for days 6 and 15 are removed to enhance readability, and related comprehensive diagrams are given in Fig. S2 in the Supplement. In addition, temporal plots for each parameter are provided in Figs. S5 (biotic) and S6 (abiotic) in the Supplement. Initial conditions of the used seawater before manipulation are as follows: $TA_{initial} \sim 2190\,\mu mol\,kg^{-1}$, $\Omega_{aragonite} \sim 2.5$–3.0, pH ~ 8.2, sal. ~ 32.6, biotic temp. 12–15 °C, and abiotic temp. 12–16 °C.

that the process would have continued if the experiment had proceeded. Despite substantial total alkalinity loss attributed to runaway precipitation, all treatments involving secondary

mineral formation still achieved a net gain in TA, ranging from 3600 to 4850 $\mu mol\,kg^{-1}$. Nevertheless, pH values in batches which underwent the precipitation process were ac-

companied by an acidification below the initial seawater pH level.

3.2 Non-CO_2-equilibrated experiments

Alkalinity enhancement in the biotic and abiotic non-CO_2-equilibrated experiments achieved a steady increase up to an addition of $2400\,\mu mol\,kg^{-1}$ at day 0 (Fig. 3). Under the given local conditions (temp. $10–11\,°C$ and sal. 32.6), exceeding the TA_{target} level of $4570\,\mu mol\,kg^{-1}$ led to a drop back to $4450 \pm 60\,\mu mol\,kg^{-1}$ after $\sim 3\,min$, irrespective of the quantity of further added alkalinity. For the biotic non-CO_2-equilibrated approach (Fig. 3a–c), treatments from ΔTA 1400 to 2800 showed a decrease in alkalinity during the subsequent 25 d run time, as a consequence of secondary mineral formation. The precipitation process uniformly came to halt in a range of $1230 \pm 60\,\mu mol\,kg^{-1}$, corresponding to an $\Omega_{aragonite}$ of 4–5. A similar behavior was observed in the abiotic non-CO_2-equilibrated experiment (Fig. 3d–f). Slightly higher water temperatures ($11–13\,°C$) in comparison to the biotic approach ($10–11\,°C$) potentially led to an earlier decline in alkalinity and a lower final TA ($1030 \pm 60\,\mu mol\,kg^{-1}$) and $\Omega_{aragonite}$ (2.5–4). All treatment levels from ΔTA 1200 to 3400 showed precipitation during the 25 d run time. Unlike the abiotic CO_2-equilibrated approach, the runaway precipitation in both non-equilibrated experiments resulted in a net loss of alkalinity, while pH values remained in the range of 9.0–10.1. Nevertheless, despite relatively high $\Omega_{aragonite}$ values of up to ~ 17 (biotic) and ~ 15 (abiotic) in the non-CO_2-equilibrated experiments, after 25 d the alkalinity was still constant in all treatments below ΔTA 1200.

3.3 TA : DIC diagrams

TA : DIC diagrams in Fig. 4a–e provide a contextualized overview of the trend and temporal development of carbonate chemistry parameters. Simultaneous TA and DIC enhancement in the CO_2-equilibrated experiments led to the characteristic diagonal gradient, while non-CO_2-equilibrated approaches resulted in a straight vertical increase in TA as a consequence of OH^- injection (also see Fig. 1). Treatments exhibiting secondary carbonate formation followed the strict 2 : 1 $\Delta TA : \Delta DIC$ decline ratio during the precipitation phase, leading to a consistent alignment of data points in straight trend trajectories. The tendency for consistent linear trends in TA/DIC during alkalinization and precipitation processes in the conducted experiments allows us to visually trace the origin of shapes and temporal development trends of pH and $\Omega_{aragonite}$ in Figs. 2 and 3 by utilizing exhibited TA : DIC diagrams. For example, the consistency of $\Omega_{aragonite}$ values within treatments that underwent the runaway process allows us to predict the final state of other carbonate chemistry parameters, oriented on the shape and position of the related $\Omega_{aragonite}$ contour (see Fig. 4b–e). The

immediate drop back to $4450 \pm 60\,\mu mol\,kg^{-1}$ in both non-CO_2-equilibrated experiments showed a consistent pattern in the dislocation of target and measured TA and DIC values. This pattern followed a steadily declining $\Delta TA : \Delta DIC$ loss ratio of 4.9–2.3 from highest to lowest target alkalinity levels (Fig. 4f), indicating the formation of non-carbonate-bearing secondary phases, such as $Mg(OH)_2$ (also see Sect. 4.3).

3.4 TA loss rates

TA loss rates for treatments which underwent the precipitation process exhibited similar relationships, independent of the CO_2 equilibration state. In regular patterns, elevated initial TA levels induced an earlier initiation of the exponential decay process accompanied by increased TA loss rates within each experiment (see Figs. 5 and S9). Absolute rates were dependent on the potential for TA loss within each treatment, regulated by the initial DIC and $\Omega_{aragonite}$ values. Irrespective of the initial TA level, treatments that showed an immediate precipitation in both non-CO_2-equilibrated experiments exhibited almost identical development trends during the precipitation process. Figure 6 showcases the related temporal TA development of the abiotic CO_2-equilibrated and biotic non-CO_2-equilibrated approaches. Outlier values from a few sampling days were excluded for the calculation of TA loss rates in the abiotic CO_2-equilibrated and abiotic non-CO_2-equilibrated experiments. For details, see section "Outliers" in the Supplement.

3.5 SEM

SEM images of the filtered residua of the experiments show a variety of common shapes of aragonite precipitates. Throughout all conducted experiments in this study, visual identifiable precipitates only appeared in treatments which also exhibited a decline in TA. The morphologies of the particles in the CO_2-equilibrated and non-CO_2-equilibrated treatments were identical if secondary mineral formation was triggered. The quantity, structures, and shapes of the particles evolved with increased alkalinity. Figure 7 provides examples of different development stages over the run time of 6 d in the non-CO_2-equilibrated biotic experiment. The bulk of particles showed central stems, which branched out to each end. Morse et al. (2007) described the more developed shapes as "broccoli" structures, due to their physical appearance, while Nielsen et al. (2014) described the less branched shapes as a "sheaf-of-wheat" bundle. These symmetric particles were the dominant shapes that appeared in secondary phases. Treatment levels with initial precipitation showed early stages of stem-like structures with very little or no branching. With higher alkalinity addition, more advanced shapes and sizes were predominant, characterized by progressive outbranching. Most developed stages exhibited a merging of the fanned-out ends to form closed spheres. Next to the dominant simple
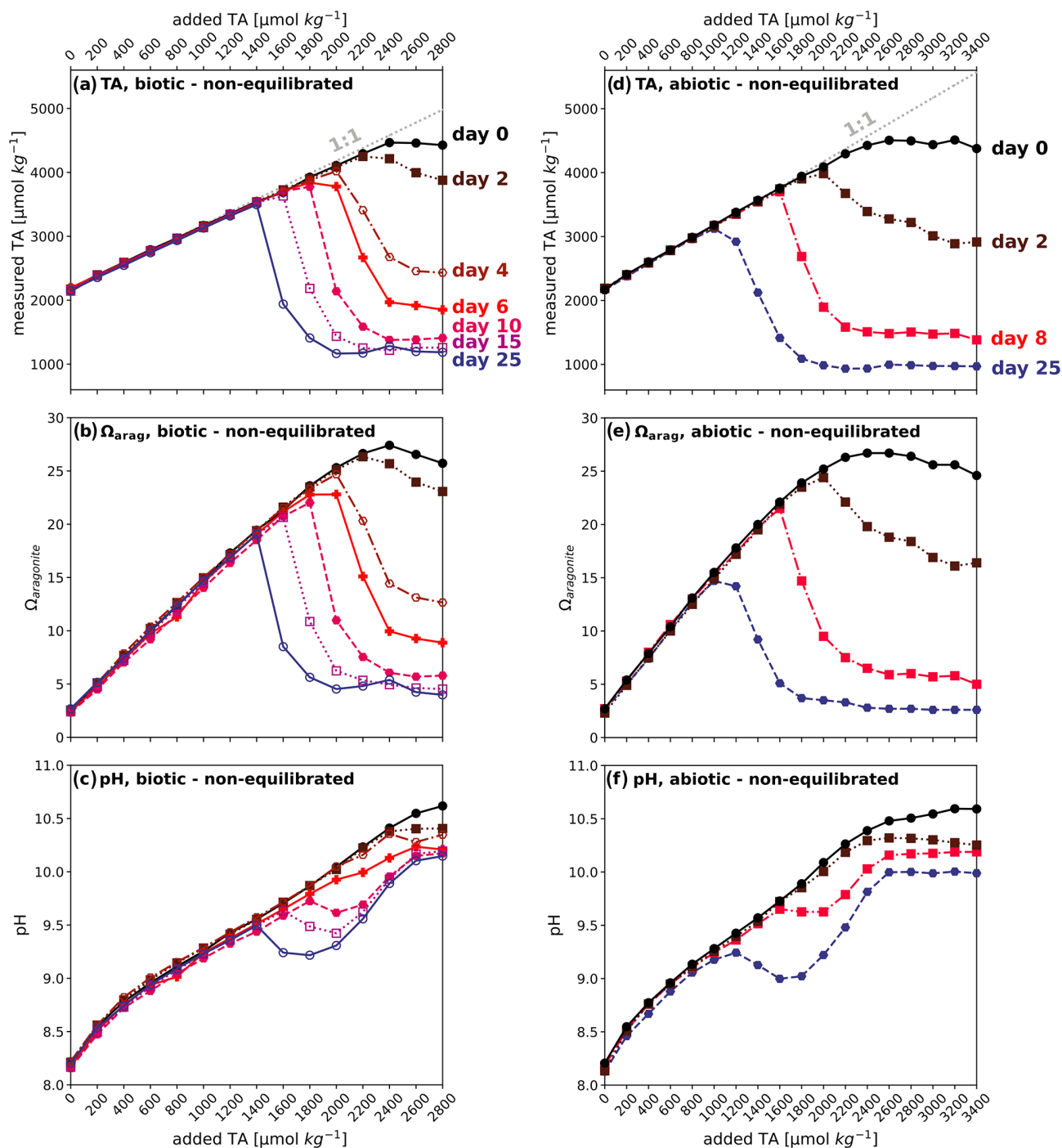
Figure 3. TA, $\Omega_{\text{aragonite}}$, and pH evolution of non-CO_2-equilibrated experiments: biotic **(a–c)** and abiotic **(d–f)**. Each graph represents a specific sampling day; due to the extensive number of data points, days 1 and 20 for the biotic treatments are removed to enhance readability. For the abiotic approach, only a subset of data is shown. Comprehensive diagrams are given in Fig. S3 in the Supplement; in addition, temporal plots for each parameter are provided in Figs. S7 (biotic) and S8 (abiotic) in the Supplement. Initial conditions of the used seawater before manipulation are as follows: TA$_{\text{initial}}$ $\sim$ 2190 µmol kg^{-1}, $\Omega_{\text{aragonite}}$ $\sim$ 2.5–3.0, pH $\sim$ 8.2, sal. $\sim$ 32.6, biotic temp. $\sim$ 10–11 °C, and abiotic temp. $\sim$ 11–13 °C.
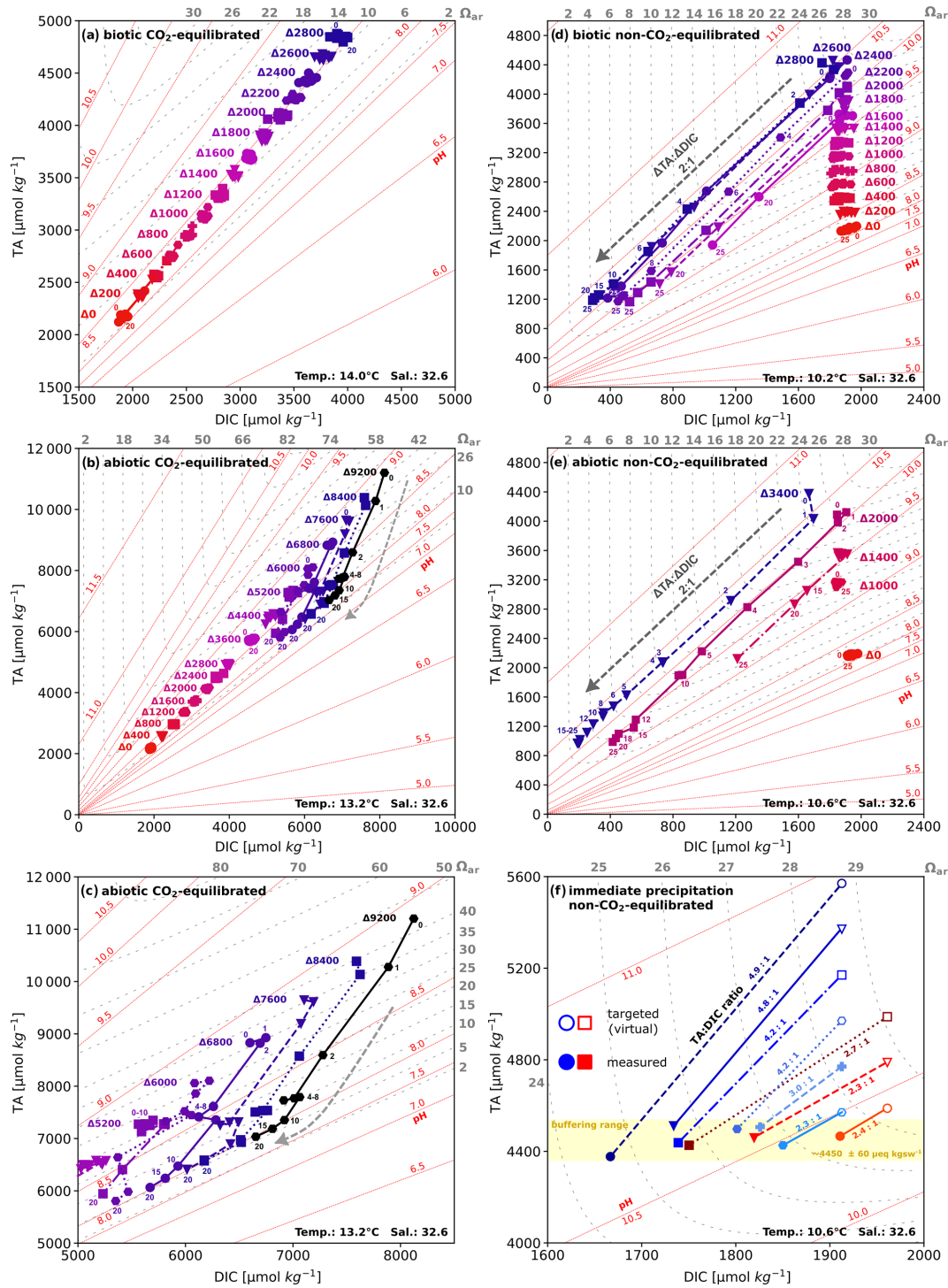
Figure 4. TA : DIC diagrams. **(a)** CO_2-equilibrated (biotic) and **(b)** CO_2-equilibrated (abiotic). **(c)** A zoom into precipitating treatments in panel **(b)**. **(d)** Non-CO_2-equilibrated (biotic) and **(e)** non-CO_2-equilibrated (abiotic). Due to the extensive number of data points within the abiotic non-CO_2-equilibrated approach, only select treatment levels are shown. A complete overview is provided in Fig. S4 in the Supplement, and select data points are labeled with their corresponding sampling days. **(f)** Comparison of targeted (hollow) and measured (filled) values for non-CO_2-equilibrated treatments with immediate precipitation, representing abiotic (blue) and biotic (red) treatments, indicating the formation of a non-carbonate phase such as $Mg(OH)_2$. Note that, due to varying temperatures during the experiments and given the $\Omega_{\text{aragonite}}$ and pH contours in all diagrams are temperature- and salinity-dependent, there may be slight inaccuracies in showing exact values for individual data points.
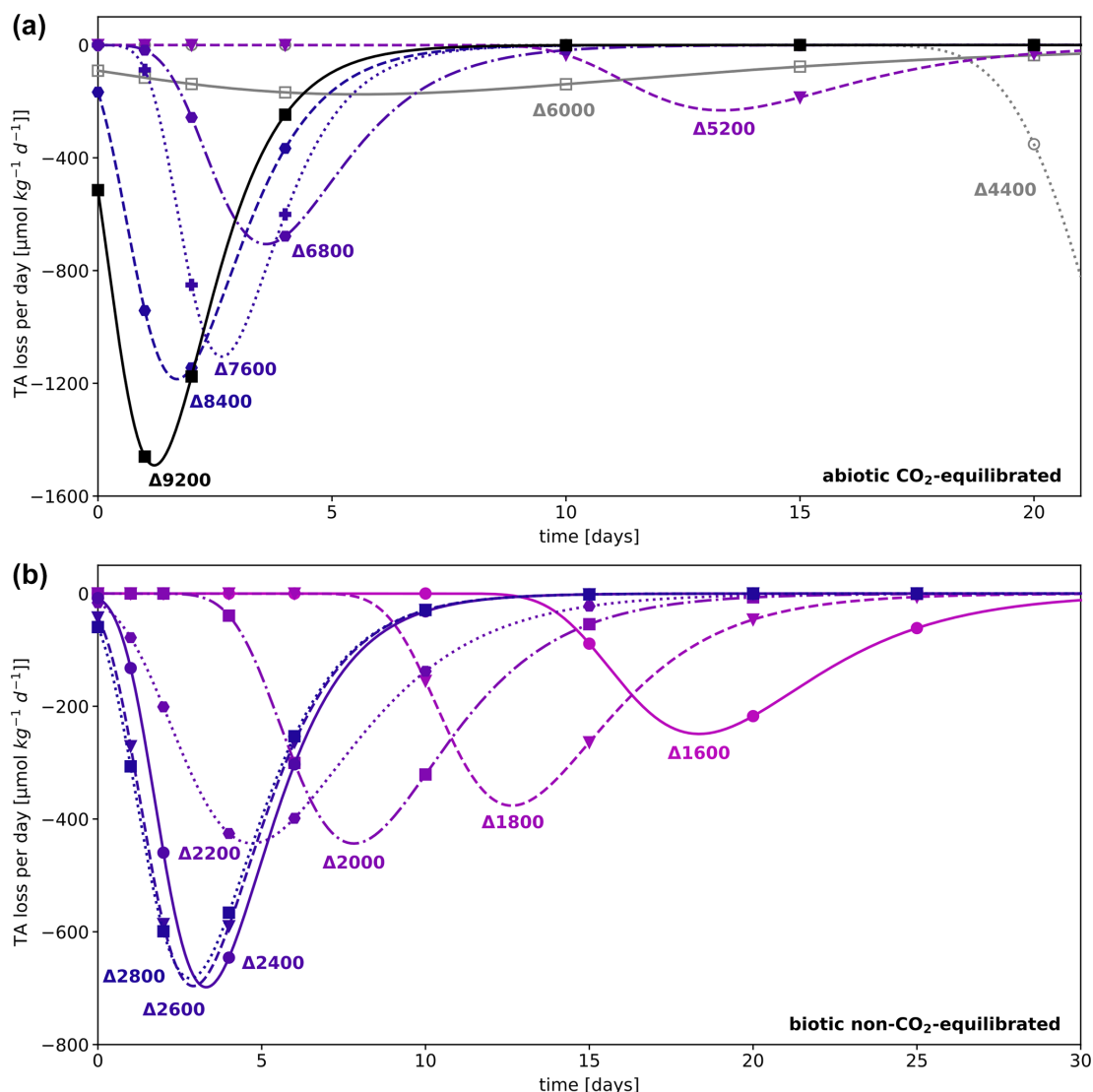
Figure 5. TA loss rates per day in **(a)** abiotic CO_2-equilibrated and **(b)** biotic non-CO_2-equilibrated experiments showing precipitation processes. Rates were calculated based on differentiating functions determined by a sigmoidal curve fit model of the temporal development of TA (see Fig. 6); due to missing data points, rates for treatment levels $\Delta4400$ and $\Delta6000$ in panel **(a)** could not be determined. Regarding ΔTA6000, see the description of outliers in the Supplement; for TA loss rates of the abiotic non-CO_2-equilibrated experiment, see Fig. S7.

stems, multipolar particles with up to six branches were observed at all development stages. Despite the variable initial branching numbers, the growth behavior followed the same patterns. Following the scheme presented in Fig. 7, all variants finally reached a closed structure. Observed ellipsoid-shaped particles might indicate that the previous precipitate was bipolar, while more spherical ones had a multipolar origin. No indications for hollow stems, as described in Hartmann et al. (2023), could be observed. Sizes vary from 2–5 µm for initial shapes to 10–30 µm for non-closed "broccoli" particles and up to 80 µm for complete spherical forms. For an overview of the occurrence and distribution of particle sizes and shapes, see Fig. 8a–f. Consistently higher loss of TA during the runaway process resulted in

greater numbers and more developed stages in the precipitates. EDX analysis uniformly identified the precipitates as Ca-dominated carbonates (Ca: 8.39 ± 2.06 mol %, Mg: 4.07 ± 0.98 mol %, Na: 0.65 ± 0.16 mol %, C: 20.41 ± 1.10 mol %, O: 64.8 ± 2.11 mol %, and Cl: 0.47 ± 0.05 mol %; median $\pm$ half-IQR, ZEISS Gemini Ultra55 Plus (CAU)) with indications of a relatively high content of Mg carbonate phases.

4 Discussion

The stability of achieved TA enhancements varied from several hours to weeks, depending primarily on the resulting
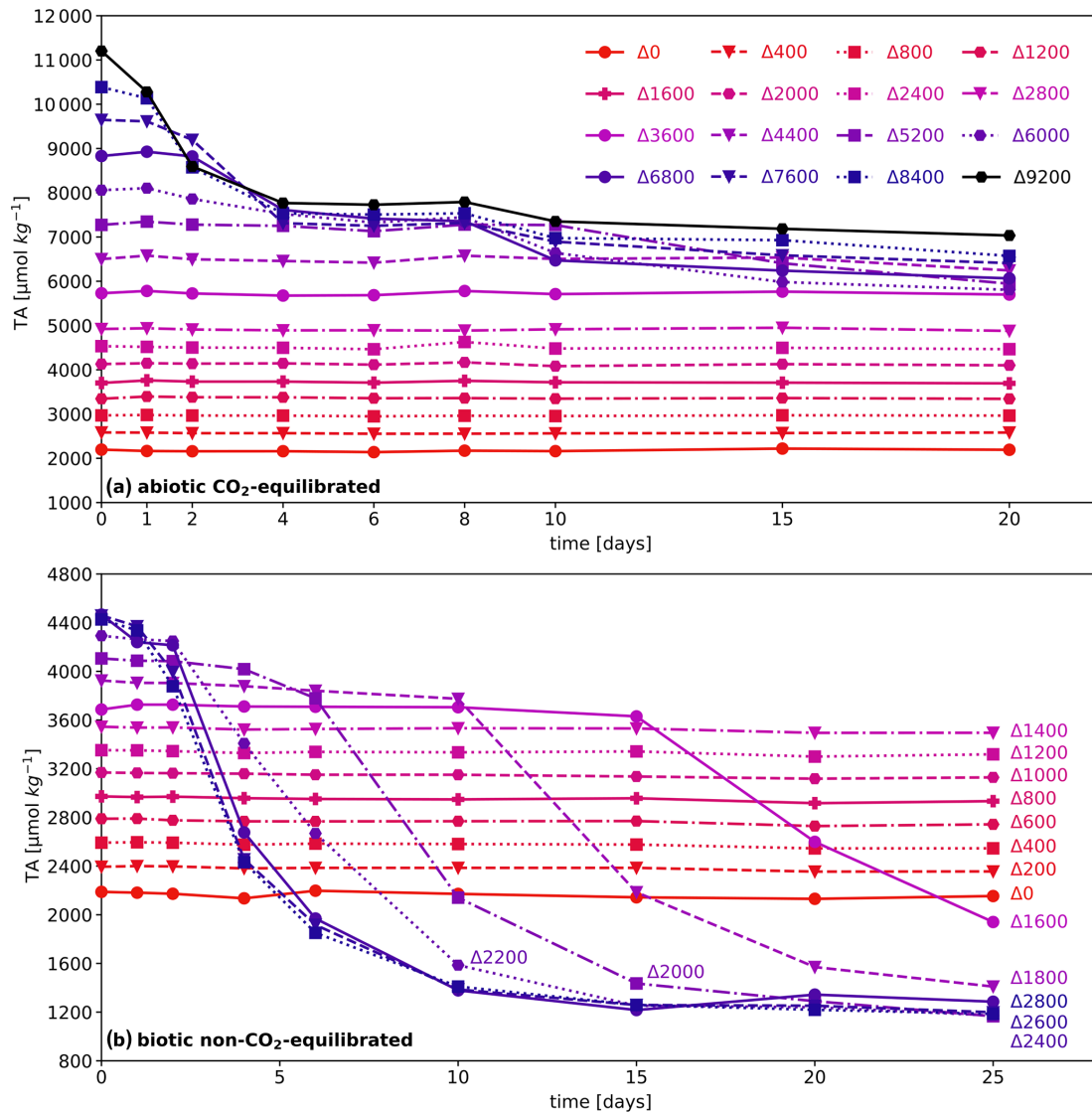
Figure 6. Temporal development of TA in **(a)** abiotic CO_2-equilibrated approaches and **(b)** biotic non-CO_2-equilibrated experiments; compare to related TA loss rates in Fig. 5. Temporal plots for each experiment are provided in the Supplement (Figs. S5–S8).

$\Omega_{aragonite}$, the CO_2 equilibration state, local environmental conditions, and the quantity of introduced alkalinity. While target TA levels were achieved within acceptable tolerances, treatment levels exceeding pH values of approximately 10.3 failed to achieve the intended TA values when measured within 3 min after application. Such observation is potentially the result of immediate magnesium hydroxide formation, buffering the injected alkalinity, as indicated by Eisaman et al. (2023) and Cyronak et al. (2023). While runaway calcium carbonate formation was demonstrated in previous research (Moras et al., 2022; Hartmann et al., 2023), a systematic description of TA loss with respect to time and saturation state could be established here. This allows the prediction of TA loss behavior when local environmental parameters are well defined. Consequently, such system-

atic studies will provide needed parameterized functions for models to assess the consequences of OAE before application (Fennel et al., 2023). Together with addressing the mixing of treated and untreated water, ultimately diluting the additional seawater TA, an assessment of the stability of alkalinity could be generated if sufficient systematic studies were conducted. Remarkably, in the CO_2-equilibrated approach for additions of up to $3600\,\mu mol\,kg^{-1}$, no TA loss was observed within the first 20 d, highlighting the relevance of the equilibration state of the carbonate system for the stability of alkalinity.
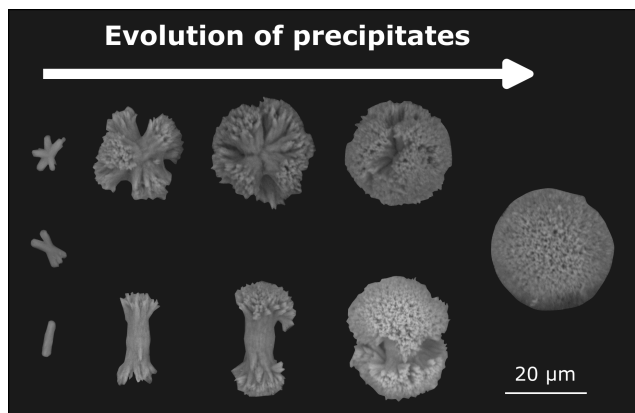
Figure 7. Scheme of the evolution of precipitates, showing a selection of precipitated particles in different development stages. Growth of the initial "stem" structure is accompanied by outbranching on each end. Independent of the polarity of the initial stems, developed particles uniformly form spherical shapes. Hitachi tabletop microscope TM4000Plus (UHH).

4.1 Runaway CaCO$_3$ precipitation

While the objective of this study was to detect stable alkalinity ranges, exceeding critical limits caused runaway carbonate formation, which leveled out at a new equilibrium. EDX analysis of the precipitates (see Sect. 3.5) and the 2 : 1 ΔTA : ΔDIC decline ratios (Fig. 4) confirmed the formation of CaCO$_3$ phases when pH values were below 10.3.

Independent of the CO$_2$ equilibration state or initial treatment level, the temporal TA development patterns after the start of runaway precipitation could be fitted with a sigmoidal function. The start of runaway precipitation, TA loss rate, and duration of TA decline (Figs. 2–6) varied with temperature and initial TA and DIC treatment levels but followed a general pattern (see Fig. 9):

1. Nucleation phase – stage of generation or provision of sufficient surface area to trigger the runaway process

2. Precipitation phase – stage of exponential decay in TA and DIC in a 2 : 1 ratio, due to the runaway process, until the potential declines significantly with reduced $\Omega_{aragonite}$ values

3. New equilibrium – final state after the runaway process ended, where the changes in TA and DIC might be too low to be measured.

4.1.1 Nucleation phase

The duration of the nucleation phase varies depending on the quantity and form of added alkalinity and on the alterations in the saturation state in this work, ranging from immediate precipitation to several weeks. However, the nucleation phase might last as long as thousands of years (cf. Pytkowicz, 1973). To date, only a small amount of data is available to
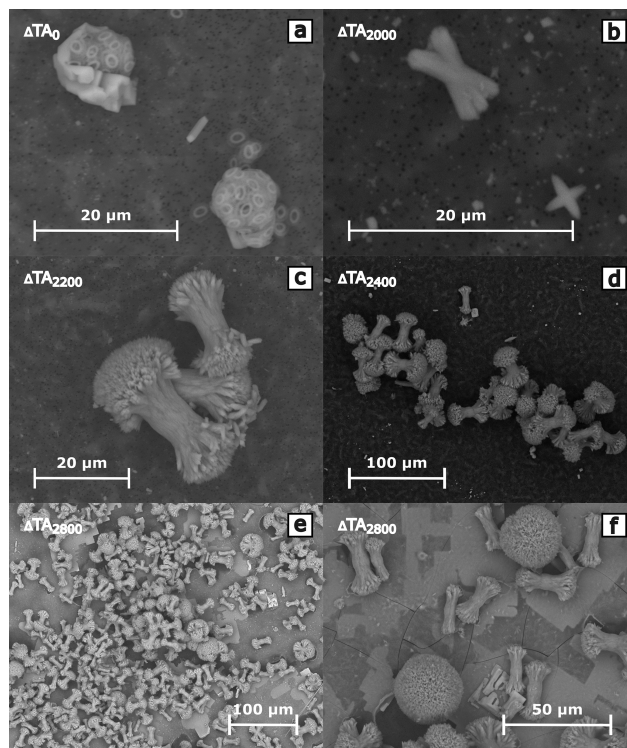

Figure 8. SEM images, overview of shapes, and occurrences of precipitates in the biotic non-CO$_2$-equilibrated treatments. No difference could be determined in shape and appearance within other experiments; compare to Boon et al. (2020), Morse et al. (1997), Pan et al. (2021), Nielsen et al. (2014), and Hartmann et al. (2023), who showed similar-shaped carbonate/aragonite precipitate. Hitachi tabletop microscope TM4000Plus (UHH).

parameterize the duration of this phase systematically. These data are needed for models to assess the consequences of OAE applications (Fennel et al., 2023).

Other factors that were not studied here, such as temperature or the presence of suitable surfaces for pseudo-homogeneous or heterogeneous precipitation, have an influence on the duration of the nucleation phase and have been suggested as triggers for CaCO$_3$ precipitation. These suitable surfaces can include but are not limited to fluvial or marine resuspended particles (Wurgaft et al., 2021, 2016), seafloor sediments (e.g., CaCO$_3$, quartz particles; Moras et al., 2022), small biotic and abiotic particles ($< 50 \, \mu$m) (Hartmann et al., 2023), seagrass, shells, biofilms, and biological activity (Aloisi et al., 2006, Zhu and Dittrich, 2016).

Dissolving alkaline particles like Ca(OH)$_2$ or Mg(OH)$_2$ for OAE could also serve as a starting point for carbonate formation (Moras et al., 2022; Hartmann et al. 2023). When relying on solid alkaline materials, Moras et al. (2022) and Schulz et al. (2023) suggested that an $\Omega_{aragonite}$ of 5 should not be exceeded, above which CaCO$_3$ runaway precipitation appears to be triggered. However, under the conditions of this study, i.e., with liquid alkaline material, the $\Omega_{aragonite}$ thresh-
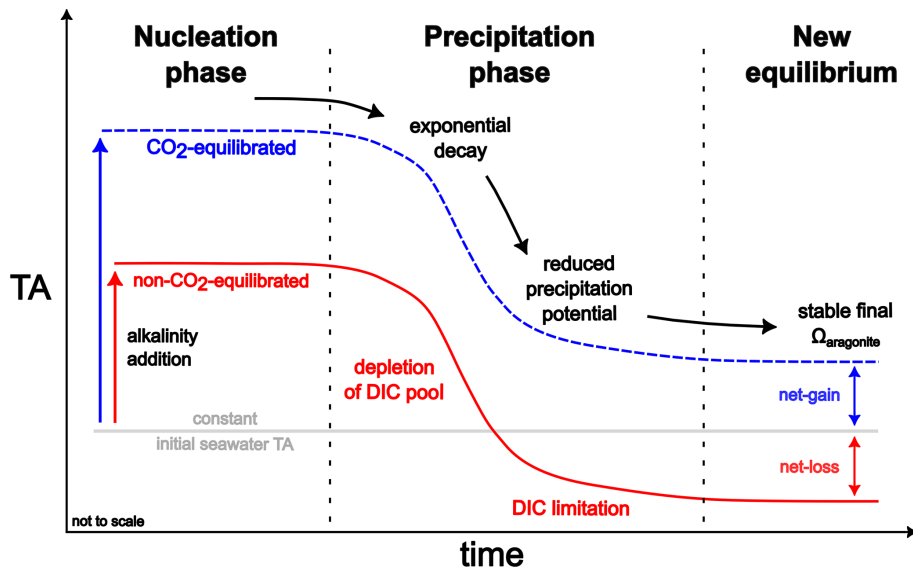
Figure 9. Concept of carbonate runaway precipitation, showing the generalized evolution of TA for non-CO_2-equilibrated and CO_2-equilibrated alkalinity addition scenarios, deduced from experimental results of this study (not to scale). As nucleation is a time-dependent process, despite overcritical $\Omega_{aragonite}$ values, a stable temporal state without observable precipitation exists, depending on the physicochemical conditions, ranging from seconds to years. While the secondary carbonate formation in the non-CO_2-equilibrated treatments results in TA values below the initial seawater levels, CO_2-equilibrated treatments might, despite a substantial TA loss during the runaway process, achieve a net gain in alkalinity. For further descriptions, see the text.

old for the initiation of spontaneous pseudo-homogeneous carbonate formation in particle-free seawater is approximately 11.3 at a salinity of 32.6 and $\sim 11\,°C$ (Marion et al., 2009, based on data from Morse and He, 1993). Most ocean surface waters are naturally oversaturated with carbonates ($\Omega_{aragonite} \sim 2$–5; Olsen et al., 2019), yet no obvious spontaneous inorganic carbonate formation occurs, as the presence of Mg^{2+} (Berner, 1975; Pan et al., 2021), phosphate (Burton and Walter, 1990), and dissolved organic matter species (Chave and Suess, 1970; Kellock et al., 2022) is known to delay or inhibit precipitation of $CaCO_3$. Since Mg^{2+} in an open-ocean context correlates to salinity, its concentration could vary depending on the local conditions (Moras et al., 2023), while phosphate and DOM concentrations are related to biological processes and seasonal changes.

4.1.2 Runaway precipitation phase: general patterns

The precipitation phase, characterized by the previously discussed parameters guiding the runaway patterns, might also be influenced by the concentration and quality of formed particles. In contrast to a natural open-ocean environment, where precipitates could sink and be removed from the alkalinity-enhanced water, the experimental setup here did not take this into account.

It is imperative to investigate if the particle export mechanism could affect the shape of the identified runaway precipitation patterns, e.g., by lower TA loss rates due to fewer suitable surface areas available for carbonate formation. The

experiments in this study were performed in bottles, where the presence of precipitation became evident through a fine whitish coating forming on the inner surface of the water-exposed part of the bottles. Despite being a laboratory artifact, the abundant presence of suspended particles suggests that, in the open ocean, similar precipitation patterns could occur. The observation of crystal growth on the bottle walls suggests that the results here and the functional relationships of the runaway precipitation might be impacted by the experimental setup, leading to higher precipitation rates due to increased potential for TA loss. Therefore, field experiments addressing this issue and confirming or improving the parameterization of the loss functions are recommended.

In natural settings, comparable TA decline patterns were observed in river plumes with high degrees of suspended particles (Wurgaft et al., 2021; 2016) or whiting events on the Great Bahama Bank (Broecker and Takahashi, 1966; Morse et al., 2003). One study suggested that, with thermohaline stratification and moderate background saturation states in an open-water column, TA loss due to carbonate formation may happen because of the strong evaporation of water in the eastern Mediterranean Sea (Bialik et al., 2022). The observation that runaway events could occur naturally under certain constrained conditions highlights the importance of identifying underlying processes before OAE applications are implemented, as the higher saturation states induced by OAE could make such events more likely.

While the fundamental patterns of changes in the carbonate system parameters during the runaway process were dic-

tated by carbonate formation, the start and end points of the procedure were dependent on the initial TA/DIC configuration and the resulting $\Omega_{aragonite}$ achieved through manipulation. The observed differences in TA loss in CO_2-equilibrated and non-CO_2-equilibrated approaches were therefore expected. Under well-defined circumstances and with an awareness of a practical final $\Omega_{aragonite}$ saturation state range, the consequences of a completed runaway precipitation process should therefore, in theory, be predictable.

As shown in Fig. 2–4, treatments which underwent a runaway process approached relatively uniform final $\Omega_{aragonite}$ values, indicating that Ω values served as the decisive factor in delineating the termination of the runaway precipitation process. Including results from this work, runaway precipitation processes in natural or artificial seawater in comparable studies (Moras et al., 2022; Hartmann et al., 2023; Fuhr et al., 2022; Pan et al., 2021) approached final $\Omega_{aragonite}$ values between 1.5 and 5.0. The variations in the final $\Omega_{aragonite}$ across the different approaches could be attributed to differences in framework conditions, such as temperature, salinity, CO_2 equilibration state, agitation methods, and sediment concentration during the course of the experiments.

4.1.3 CO_2 equilibration states

While the precipitation rates in this study decreased significantly at the end of each experiment, approaching $\Omega_{aragonite}$ values of 2.5–5.0, it cannot be excluded that further formation of secondary phases could have continued. While some treatments within the non-CO_2-equilibrated experiments still experienced a daily decline of $1–10\,\mu mol\,kg^{-1}$ in TA during the last 5 d of operation, these changes were relatively insignificant compared to their earlier rates. Nonetheless, slight changes were still observed, and it cannot be ruled out that the process stopped after a run time of 25 d.

In contrast to the non-CO_2-equilibrated approach, the CO_2-equilibrated experiments showed relatively constant final $\Omega_{aragonite}$ values of 5.8–6.0 at the end of the abiotic experiments after 20 d. The runaway process is anticipated to persist at lower levels of TA loss rates, given that they consistently declined by $20–30\,\mu mol\,kg^{-1}\,d^{-1}$ during the final 5 d of operation.

4.1.4 Comparison to other experiments

Time spans to reach the end of the runaway precipitation process in studies with comparable setups, solely focusing on non-CO_2-equilibrated treatments with a ΔTA_{added} of $2000\,\mu mol\,kg^{-1}$, ranged from 4 d in Hartmann et al. (2023) to more than 14 d in Moras et al. (2022). In Moras et al. (2022), there were variations in the experimental conditions, such as the use of solid $Ca(OH)_2$ for TA enhancement, constant agitation, and a temperature of 21 °C. These differences may hinder a direct comparison with our study. By contrast, this study employed the configuration introduced by Hart-

mann et al. (2023), with the only distinction being the utilization of seawater with a salinity of 36.2 and a temperature of around 23 °C. In this study, with a salinity of 32.6 and temperatures ranging from 10 to 16 °C, the precipitation process in the highest treatments came close to a halt after $\sim 15\,d$ in the non-CO_2-equilibrated approaches, while alkalinity was stable over 20 d in CO_2-equilibrated treatments with ΔTA_{added} up to $3600\,\mu mol\,kg^{-1}$. However, in the Hartmann et al. (2023) experiments, significantly faster precipitation rates were observed. This underscores the crucial influence of local environmental factors and the application scenario in shaping the dynamics of the runaway process.

Following the Ω threshold described by Marion et al. (2009) and experimental results from Pytkowicz (1973), and considering the general trend predictions from the TA loss rates (Fig. 5), it is suggested that further treatments in this study might have initiated the runaway process if the experiments had continued. Therefore, treatment levels above $\Delta TA600\,\mu mol\,kg^{-1}$ in the non-CO_2-equilibrated and $\Delta TA2400\,\mu mol\,kg^{-1}$ in CO_2-equilibrated approaches had the potential to start carbonate precipitation.

As manipulated water parcels in real-world application scenarios would be diluted by untreated water, the results of our study suggest a functional relationship with time for the dilution of TA-enhanced water to non-critical $\Omega_{aragonite}$ values. This could range from minutes to weeks (see Figs. 4 and 10) depending on the local physicochemical conditions, the CO_2 equilibration state, and the achieved TA levels. Further research is therefore needed to identify the functional relationship for other environmental settings, such as temperature and salinity, and the impact of particles for near-coastal settings. This is necessary to determine if the relationships identified here are universally valid or, in the context of OAE, if further factors need to be considered. In addition, experiments on the dilution of manipulated water masses are needed to test whether TA values exceeding critical ranges can be stabilized. By understanding patterns and factors driving the runaway process, measures could be taken to prevent unwanted consequences during TA addition.

4.2 Temporal stability after TA addition

In the context of an open-ocean application of OAE, induced turbulence and advective energy in the water would cause the mixing of the alkalized water body with untreated surrounding seawater. Specifically, ship-based applications offer the potential to significantly change the concentrations and saturation states in a relatively short amount of time (e.g., Caserini et al., 2021; He and Tyka, 2023; Renforth and Henderson, 2017). Dilution could potentially prevent or delay the nucleation phase for a significant amount of time, to a degree that runaway precipitation events can be avoided at time scales relevant for CDR.

While TA values reached in this study might not represent final targeted TA levels for a real-world application after im-
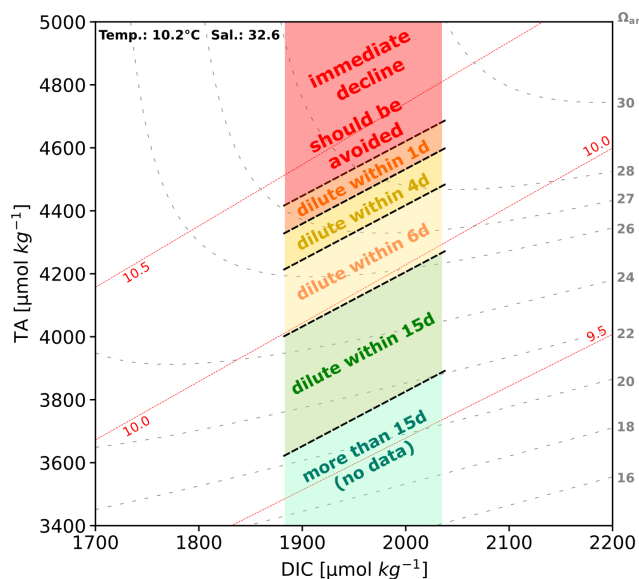
Figure 10. Stability ranges during non-CO$_2$-equilibrated experiments showing upper critical limits for application, which should be avoided to prevent runaway precipitation and its consequences. ΔTA0: TA $\sim$ 2200 μmol kg^{-1}, DIC $\sim$ 1960 μmol kg^{-1}, pH $\sim$ 8.2, temperature 10.2 °C, salinity 32.6. The red area highlights the critical zone for immediate precipitation. The tolerance times for dilution or other actions to prevent the runaway process are indicated. Ranges in this diagram are applicable only to this setting and should not be generalized.

mediate dilution with untreated water parcels, studied ranges provide experimental insight into processes during transient enhanced conditions, occurring around point sources or in (partially) enclosed water bodies without adequate mixing. Derived from the results of non-CO$_2$-equilibrated setups, Fig. 10 provides an overview of the TA ranges and time frames until which a manipulated water mass should be diluted to prevent the onset of secondary mineral formation. Note that, for the CO$_2$-equilibrated approaches, this study could not determine reliable comparable stability ranges.

As described above, treatments which reached TA levels above 4450 μmol kg^{-1} within the non-CO$_2$-equilibrated approach immediately lost parts of the added TA. To avoid any kind of secondary mineral formation under the local conditions of Raunefjorden, these values should not be surpassed without additional measures. In theory, every ocean water mass should possess such a critical threshold level for immediate precipitation. This threshold would determine the practical upper limit for the application scenarios and overall efficiency of OAE. At present, there does not seem to be a comprehensive method for calculating this upper threshold. Such a method would need to take into consideration the complexities of the natural environment, such as seasonal and biological cycles, distinct geographical characteristics, and the various approaches of TA addition. To derive such a method would need systematic research to identify

relevant factors and field trials aimed at exploring their interactions under real-world conditions. Nevertheless, results of this study also showed that TA could be enhanced above ΔTA$_{added}$ of 2000 μmol kg^{-1} in a non-CO$_2$-equilibrated style without any adverse geochemical consequences if sufficient mixing is ensured within the given local temporal stability ranges.

4.3 Immediate magnesium hydroxide precipitation

If, by addition of NaOH to seawater, a pH of 10.4 (at 21 °C) is reached, Mg(OH)$_2$ is formed. This is a long-known process described by Haas (1916) and Kapp (1928) and is comparable to values reached in this study within the non-CO$_2$-equilibrated treatments, showing an immediate TA decline (pH 10.3–10.6 at 10–12 °C). This suggests that the aforementioned process could potentially account for the immediate precipitation observed in the present experiments. As described by Turek and Gnot (1995), the formation of Mg(OH)$_2$ during this practice could be regarded as an "immediate process", which aligns with observations in this study. The buffering of TA by Mg(OH)$_2$ formation during TA injection was also supported by the ΔTA : ΔDIC change ratios of 2.3–4.9 : 1 (Fig. 4f) immediately after alkalinity addition. Co-precipitation of carbonate phases besides the generation of Mg(OH)$_2$ would be necessary to achieve these change ratios and is a regular feature in seawater (Battaglia et al., 2022; Nguyen Dang et al., 2017; Turek and Gnot, 1995). Formed solid Mg(OH)$_2$ particles could have acted as triggers for further precipitation of carbonate phases, leading to the observed earlier initiation of the runaway process.

During the injection of NaOH stock solution in seawater, the sharp gradient in pH/TA concentrations could lead to the generation of lysospheres and floccules, which aggregate and enclose water in its pore space (Turek and Gnot, 1995). Similar observations were made by Badjatya et al. (2022), who described it as colloidal suspension. While the addition levels were significantly lower in this study compared to Badjatya et al. (2022), a comparable trend after the injection was evident. This trend was visually observable across all non-CO$_2$-equilibrated treatments above ΔTA200. However, to observe the same phenomenon in the CO$_2$-equilibrated approaches, higher treatment levels (>ΔTA2000) were required to form aggregates.

In the absence of further agitation, aggregates that had formed remained visible for several days. However, when the bottles were gently rotated after TA addition, aggregates disintegrated and all treatments that were initially below the critical threshold for immediate precipitation reached their target TA levels. These observations suggest that the immediate formation of potential Mg(OH)$_2$ aggregates during the injection process might be reversible, as also noted by Cyronak et al. (2023). In a real-world scenario, wave movement and dilution processes with untreated waters might allow the redissolution of Mg(OH)$_2$ or further metastable carbonate phases.

Effects such as an increase in undesired turbidity during TA addition, as stated by Eisaman et al. (2023), might therefore be temporal. Depending on the speed of the redissolution process, sedimentation of the aggregates might function as an export factor, transferring the added alkalinity to greater depths. The enclosed water in the lysospheres might nevertheless reduce the sinking rate significantly due to its relatively low density (Turek and Gnot, 1995).

5 Conclusion

After the introduction of the runaway precipitation concept by Moras et al. (2022) and Hartmann et al. (2023), this study has identified functional relationships of TA change rates after initiation of the secondary carbonate formation process. With well-defined framework parameters of $\Omega_{aragonite}$, temperature, and salinity, it is therefore possible to predict the temporal evolution of alkalinity. Once the runaway process was triggered, patterns of TA loss were identical for both CO_2-equilibrated and non-CO_2-equilibrated TA addition approaches. While a progressing runaway process negatively impacts carbonate chemistry parameters, the observed delayed onset of detectable solid-phase formation implies that alkalinity could be enhanced beyond $2000\,\mu mol\,kg^{-1}$ when sufficient dilution with untreated water could be ensured within given time ranges. With knowledge of the local environmental conditions, introduced $\Omega_{aragonite}$, and the CO_2 equilibration state, it is hypothesized that it is possible to predict a temporary stability range for any given system. The ability to predict the outcomes in advance can facilitate environmental assessments prior to OAE applications. Furthermore, the parameters acquired could be essential for computer models to carry out these evaluations.

The seawater used in this study had low sediment concentrations; therefore, identified TA rate changes during runaway precipitation or temporary stability ranges might differ for systems with higher suspended sediment concentrations, especially if suitable crystal surfaces are abundant (cf. Moras et al., 2022; Hartmann et al., 2023). Unlike in Hartmann et al. (2023), no relevant differences between biotic and abiotic approaches (distinguished by the filter mesh size) could be identified.

For non-CO_2-equilibrated TA additions, an upper pH threshold of around 10.3 could be observed. Crossing this threshold comes with the potential consequence of magnesium hydroxide formation, which was also seen in other studies (cf. Badjatya et al., 2022; Turek and Gnot, 1995; Vassallo et al., 2021). Considerations about the TA treatment levels in open-ocean application scenarios must therefore consider the onset of $Mg(OH)_2$ formation as an upper threshold. To maximize effectiveness, it is crucial to maintain concentrations just below this critical value when injecting alkalinity into seawater, especially if the local seawater possesses efficient dilution capabilities.

These considerations are relevant for modeling the limitations and dynamics of alkalinity enhancement in the ocean, as demonstrated by He and Tyka (2023). Nevertheless, it is essential to validate these findings with in situ experiments to establish parameters and functional relationships applicable to open-ocean environments. It is only under these circumstances that accurate assessments can be made. The most promising outcome of this study is the possibility to predict abiotic processes and the stability of alkalinity for effective and realistic applications in the future.

Author contributions. The idea for this work was conceived by NS and JH. NS, GF, and CL designed the experiments with help from JH, JS, and UR. NS, CL, GF, and JS carried out sampling and laboratory analysis. NS interpreted the data with help from GF and JH. NS and JH wrote the text with contributions from all co-authors.

References

Albright, R., Caldeira, L., Hosfelt, J., Kwiatkowski, L., Maclaren, J. K., Mason, B. M., Nebuchina, Y., Ninokawa, A., Pongratz, J., Ricke, K. L., Rivlin, T., Schneider, K., Sesboüé, M., Shamberger, K., Silverman, J., Wolfe, K., Zhu, K., and Caldeira, K.: Reversal of ocean acidification enhances net coral reef calcification, Nature, 531, 362–365, https://doi.org/10.1038/nature17155, 2016.

Aloisi, G., Gloter, A., Krüger, M., Wallmann, K., Guyot, F., and Zuddas, P.: Nucleation of calcium carbonate on bacterial nanoglobules, Geology, 34, 1017–1020, https://doi.org/10.1130/g22986a.1, 2006.

Bach, L. T., Gill, S. J., Rickaby, R. E. M., Gore, S., and Renforth, P.: CO_2 Removal With Enhanced Weathering and Ocean Alkalinity Enhancement: Potential Risks and Co-benefits for Marine Pelagic Ecosystems, Frontiers in Climate, 1, 1038, https://doi.org/10.3389/fclim.2019.00007, 2019.

Badjatya, P., Akca, A. H., Fraga Alvarez, D. V., Chang, B., Ma, S., Pang, X., Wang, E., van Hinsberg, Q., Esposito, D. V., and Kawashima, S.: Carbon-negative cement manufacturing from seawater-derived magnesium feedstocks, P. Natl. Acad. Sci. USA, 119, e2114680119, https://doi.org/10.1073/pnas.2114680119, 2022.

Badocco, D., Pedrini, F., Pastore, A., di Marco, V., Marin, M. G., Bogialli, S., Roverso, M., and Pastore, P.: Use of a simple empirical model for the accurate conversion of the seawater pH value measured with NIST calibration into seawater pH scales, Talanta, 225, 122051, https://doi.org/10.1016/j.talanta.2020.122051, 2021.

Battaglia, G., Domina, M. A., Lo Brutto, R., Lopez Rodriguez, J., Fernandez de Labastida, M., Cortina, J. L., Pettignano, A., Cipollina, A., Tamburini, A., and Micale, G.: Evaluation of the Purity of Magnesium Hydroxide Recovered from Saltwork Bitterns, Water, 15, 29, https://doi.org/10.3390/w15010029, 2022.

Benthaus, F.-C., Totsche, O., and Luckner, L.: In-lake Neutralization of East German Lignite Pit Lakes: Technical History and New Approaches from LMBV, Mine Water Environ., 39, 603–617, https://doi.org/10.1007/s10230-020-00707-5, 2020.

Berner, R. A.: The role of magnesium in the crystal growth of calcite and aragonite from sea water, Geochim. Cosmochim. Ac., 39, 489–504, https://doi.org/10.1016/0016-7037(75)90102-7, 1975.

Berner, R. A., Lasaga, A. C., and Garrels, R. M.: Carbonate-silicate geochemical cycle and its effect on atmospheric carbon dioxide over the past 100 million years, Am. J. Sci., 283, 641–683, https://doi.org/10.2475/ajs.283.7.641, 1983.

Bialik, O. M., Sisma-Ventura, G., Vogt-Vincent, N., Silverman, J., and Katz, T.: Role of oceanic abiotic carbonate precipitation in future atmospheric CO_2 regulation, Sci. Rep.-UK, 12, 15970, https://doi.org/10.1038/s41598-022-20446-7, 2022.

Boon, M., Rickard, W. D. A., Rohl, A. L., and Jones, F.: Stabilization of Aragonite: Role of Mg^{2+} and Other Impurity Ions, Cryst. Growth Des., 20, 5006–5017, https://doi.org/10.1021/acs.cgd.0c00152, 2020.

Broecker, W. S. and Takahashi, T.: Calcium carbonate precipitation on the Bahama Banks, J. Geophys. Res., 71, 1575–1602, https://doi.org/10.1029/JZ071i006p01575, 1966.

Burton, E. A. and Walter, L. M.: The role of pH in phosphate inhibition of calcite and aragonite precipitation rates in seawater, Geochim. Cosmochim. Ac., 54, 797–808, https://doi.org/10.1016/0016-7037(90)90374-T, 1990.

Caldeira, K. and Rau, G. H.: Accelerating carbonate dissolution to sequester carbon dioxide in the ocean: Geochemical implications, Geophys. Res. Lett., 27, 225–228, https://doi.org/10.1029/1999gl002364, 2000.

Caserini, S., Pagano, D., Campo, F., Abbà, A., De Marco, S., Righi, D., Renforth, P., and Grosso, M.: Potential of Maritime Transport for Ocean Liming and Atmospheric CO_2 Removal, Frontiers in Climate, 3, 575900, https://doi.org/10.3389/fclim.2021.575900, 2021.

Chave, K. E. and Suess, E.: Calcium Carbonate Saturation in Seawater: Effects of Dissolved Organic Matter, Limnol. Oceanogr., 15, 633–637, https://doi.org/10.4319/lo.1970.15.4.0633, 1970.

Cyronak, T., Albright, R., and Bach, L. T.: Field experiments in ocean alkalinity enhancement research, in: Guide to Best Practices in Ocean Alkalinity Enhancement Research, edited by: Oschlies, A., Stevenson, A., Bach, L. T., Fennel, K., Rickaby, R. E. M., Satterfield, T., Webb, R., and Gattuso, J.-P., Copernicus Publications, State Planet, 2-oae2023, 7, https://doi.org/10.5194/sp-2-oae2023-7-2023, 2023.

Deffeyes, K. S.: Carbonate Equilibria: A Graphic and Algebraic Approach1, Limnol. Oceanogr., 10, 412–426, https://doi.org/10.4319/lo.1965.10.3.0412, 1965.

Dickson, A. G.: Standard potential of the reaction: AgCl(s) + $\frac{1}{2}H_2$(g) = Ag(s) + HCl(aq), and and the standard acidity constant of the ion HSO_4^- in synthetic sea water from 273.15 to 318.15 K, J. Chem. Thermodyn., 22, 113–127, https://doi.org/10.1016/0021-9614(90)90074-Z, 1990.

Eisaman, M. D., Geilert, S., Renforth, P., Bastianini, L., Campbell, J., Dale, A. W., Foteinis, S., Grasse, P., Hawrot, O., Löscher, C. R., Rau, G. H., and Rønning, J.: Assessing the technical aspects of ocean-alkalinity-enhancement approaches, in: Guide to Best Practices in Ocean Alkalinity Enhancement Research, edited by: Oschlies, A., Stevenson, A., Bach, L. T., Fennel, K., Rickaby, R. E. M., Satterfield, T., Webb, R., and Gattuso, J.-P., Copernicus Publications, State Planet, 2-oae2023, 3, https://doi.org/10.5194/sp-2-oae2023-3-2023, 2023.

Fennel, K., Long, M. C., Algar, C., Carter, B., Keller, D., Laurent, A., Mattern, J. P., Musgrave, R., Oschlies, A., Ostiguy, J., Palter, J. B., and Whitt, D. B.: Modelling considerations for research on ocean alkalinity enhancement (OAE), in: Guide to Best Practices in Ocean Alkalinity Enhancement Research, edited by: Oschlies, A., Stevenson, A., Bach, L. T., Fennel, K., Rickaby, R. E. M., Satterfield, T., Webb, R., and Gattuso, J.-P., Copernicus Publications, State Planet, 2-oae2023, 9, https://doi.org/10.5194/sp-2-oae2023-9-2023, 2023.

Ferderer, A., Chase, Z., Kennedy, F., Schulz, K. G., and Bach, L. T.: Assessing the influence of ocean alkalinity enhancement on a coastal phytoplankton community, Biogeosciences, 19, 5375–5399, https://doi.org/10.5194/bg-19-5375-2022, 2022.

Forster, M.: Investigations for the environmentally friendly production of Na_2CO_3 and HCl from exhaust CO_2, NaCl and H_2O, J. Clean. Prod., 23, 195–208, https://doi.org/10.1016/j.jclepro.2011.10.012, 2012.

Forster, M.: Investigations to convert CO_2, NaCl and H_2O into Na_2CO_3 and HCl by thermal solar energy with high solar efficiency, Journal of CO2 Utilization, 7, 11–18, https://doi.org/10.1016/j.jcou.2014.06.001, 2014.

Fuhr, M., Geilert, S., Schmidt, M., Liebetrau, V., Vogt, C., Ledwig, B., and Wallmann, K.: Kinetics of Olivine Weathering

in Seawater: An Experimental Study, Front. Clim., 4, 831587, https://doi.org/10.3389/fclim.2022.831587, 2022.

Haas, A. R.: The Effect of the Addition of Alkali to Sea Water Upon the Hydrogen Ion Concentration, J. Biol. Chem., 26, 515–517, https://doi.org/10.1016/s0021-9258(18)87433-6, 1916.

Hartmann, J., West, A. J., Renforth, P., Köhler, P., De La Rocha, C. L., Wolf-Gladrow, D. A., Dürr, H. H., and Scheffran, J.: Enhanced chemical weathering as a geoengineering strategy to reduce atmospheric carbon dioxide, supply nutrients, and mitigate ocean acidification, Rev. Geophys., 51, 113–149, https://doi.org/10.1002/rog.20004, 2013.

Hartmann, J., Suitner, N., Lim, C., Schneider, J., Marín-Samper, L., Arístegui, J., Renforth, P., Taucher, J., and Riebesell, U.: Stability of alkalinity in ocean alkalinity enhancement (OAE) approaches – consequences for durability of CO_2 storage, Biogeosciences, 20, 781–802, https://doi.org/10.5194/bg-20-781-2023, 2023.

He, J. and Tyka, M. D.: Limits and CO_2 equilibration of near-coast alkalinity enhancement, Biogeosciences, 20, 27–43, https://doi.org/10.5194/bg-20-27-2023, 2023.

Ilyina, T., Six, K. D., Segschneider, J., Maier-Reimer, E., Li, H., and Núñez-Riboni, I.: Global ocean biogeochemistry model HAMOCC: Model architecture and performance as component of the MPI-Earth system model in different CMIP5 experimental realizations, J. Adv. Model. Earth Sy., 5, 287–315, https://doi.org/10.1029/2012ms000178, 2013.

Kapp, E. M.: The precipitation of calcium and magnesium from sea water by sodium hydroxide, Biol. Bull., 55, 453–458, 1928.

Kellock, C., Castillo Alvarez, M. C., Finch, A., Penkman, K., Kroger, R., Clog, M., and Allison, N.: Optimising a method for aragonite precipitation in simulated biogenic calcification media, PLOS One, 17, e0278627, https://doi.org/10.1371/journal.pone.0278627, 2022.

Kheshgi, H. S.: Sequestering atmospheric carbon dioxide by increasing ocean alkalinity, Energy, 20, 915–922, https://doi.org/10.1016/0360-5442(95)00035-F, 1995.

Koch, C. and Manzur, K.: A new technology of pit lake treatment using calcium oxide and carbon dioxide to increase alkalinity, IMWA 2016 – Mining Meets Water – Conflicts and Solutions, 11–15 July 2016, Leipzig, Germany, Technische Universität Bergakademie Freiberg, International Mine Water Association, 284–229, ISBN 978-3-86012-533-5, 2016.

Köhler, P., Hartmann, J., and Wolf-Gladrow, D. A.: Geoengineering potential of artificially enhanced silicate weathering of olivine, P. Natl. Acad. Sci. USA, 107, 20228–20233, https://doi.org/10.1073/pnas.1000545107, 2010.

Lee, K., Kim, T.-W., Byrne, R. H., Millero, F. J., Feely, R. A., and Liu, Y.-M.: The universal ratio of boron to chlorinity for the North Pacific and North Atlantic oceans, Geochim. Cosmochim. Ac., 74, 1801–1811, https://doi.org/10.1016/j.gca.2009.12.027, 2010.

Lueker, T. J., Dickson, A. G., and Keeling, C. D.: Ocean pCO_2 calculated from dissolved inorganic carbon, alkalinity, and equations for K1 and K2: validation based on laboratory measurements of CO_2 in gas and seawater at equilibrium, Mar. Chem., 70, 105–119, https://doi.org/10.1016/S0304-4203(00)00022-0, 2000.

Mackenzie, F. T. and Garrels, R. M.: Chemical mass balance between rivers and oceans, Am. J. Sci., 264, 507–525, https://doi.org/10.2475/ajs.264.7.507, 1966.

Marion, G. M., Millero, F. J., and Feistel, R.: Precipitation of solid phase calcium carbonates and their effect on application of seawater S_A–T–P models, Ocean Sci., 5, 285–291, https://doi.org/10.5194/os-5-285-2009, 2009.

Meinshausen, M., Meinshausen, N., Hare, W., Raper, S. C., Frieler, K., Knutti, R., Frame, D. J., and Allen, M. R.: Greenhouse-gas emission targets for limiting global warming to 2 °C, Nature, 458, 1158–1162, https://doi.org/10.1038/nature08017, 2009.

Moras, C., Bach, L., Cyronak, T., Joannes-Boyau, R., and Schulz, K.: Effects of grain size and seawater salinity on brucite dissolution and secondary calcium carbonate precipitation kinetics: implications for Ocean Alkalinity Enhancement, EGU General Assembly 2023, Vienna, Austria, 24–28 Apr 2023, EGU23-330, https://doi.org/10.5194/egusphere-egu23-330, 2023.

Moras, C. A., Bach, L. T., Cyronak, T., Joannes-Boyau, R., and Schulz, K. G.: Ocean alkalinity enhancement – avoiding runaway $CaCO_3$ precipitation during quick and hydrated lime dissolution, Biogeosciences, 19, 3537–3557, https://doi.org/10.5194/bg-19-3537-2022, 2022.

Morse, J. W. and He, S.: Influences of T, S and P_{CO_2} on the pseudo-homogeneous precipitation of $CaCO_3$ from seawater: implications for whiting formation, Mar. Chem., 41, 291–297, https://doi.org/10.1016/0304-4203(93)90261-L, 1993.

Morse, J. W., Wang, Q., and Tsio, M. Y.: Influences of temperature and Mg: Ca ratio on CaCO3 precipitates from seawater, Geology, 25, 85–87, https://doi.org/10.1130/0091-7613(1997)025<0085:IOTAMC>2.3.CO;2, 1997.

Morse, J. W., Gledhill, D. K., and Millero, F. J.: Caco3 precipitation kinetics in waters from the great Bahama bank, Geochim. Cosmochim. Ac., 67, 2819–2826, https://doi.org/10.1016/s0016-7037(03)00103-0, 2003.

Morse, J. W., Arvidson, R. S., and Lüttge, A.: Calcium carbonate formation and dissolution, Chem. Rev., 107, 342–381, https://doi.org/10.1021/cr050358j, 2007.

NASEM: A Research Strategy for Ocean-based Carbon Dioxide Removal and Sequestration, National Academies of Sciences, Engineering, and Medicine, Washington, DC, https://doi.org/10.17226/26278, 2022.

Nguyen Dang, D., Gascoin, S., Zanibellato, A., G. Da Silva, C., Lemoine, M., Riffault, B., Sabot, R., Jeannin, M., Chateigner, D., and Gil, O.: Role of brucite dissolution in calcium carbonate precipitation from artificial and natural seawaters, Cryst. Growth Des., 17, 1502–1513, https://doi.org/10.1021/acs.cgd.6b01305, 2017.

Nielsen, M. H., Aloni, S., and De Yoreo, J. J.: In situ TEM imaging of $CaCO_3$ nucleation reveals coexistence of direct and indirect pathways, Science, 345, 1158–1162, https://doi.org/10.1126/science.1254051, 2014.

Olsen, A., Lange, N., Key, R. M., Tanhua, T., Álvarez, M., Becker, S., Bittig, H. C., Carter, B. R., Cotrim da Cunha, L., Feely, R. A., van Heuven, S., Hoppema, M., Ishii, M., Jeansson, E., Jones, S. D., Jutterström, S., Karlsen, M. K., Kozyr, A., Lauvset, S. K., Lo Monaco, C., Murata, A., Pérez, F. F., Pfeil, B., Schirnick, C., Steinfeldt, R., Suzuki, T., Telszewski, M., Tilbrook, B., Velo, A., and Wanninkhof, R.: GLODAPv2.2019 –

an update of GLODAPv2, Earth Syst. Sci. Data, 11, 1437–1461, https://doi.org/10.5194/essd-11-1437-2019, 2019.

Orr, J. C., Epitalon, J.-M., Dickson, A. G., and Gattuso, J.-P.: Routine uncertainty propagation for the marine carbon dioxide system, Mar. Chem., 207, 84–107, https://doi.org/10.1016/j.marchem.2018.10.006, 2018.

Oschlies, A., Bach, L. T., Rickaby, R. E. M., Satterfield, T., Webb, R., and Gattuso, J.-P.: Climate targets, carbon dioxide removal, and the potential role of ocean alkalinity enhancement, in: Guide to Best Practices in Ocean Alkalinity Enhancement Research, edited by: Oschlies, A., Stevenson, A., Bach, L. T., Fennel, K., Rickaby, R. E. M., Satterfield, T., Webb, R., and Gattuso, J.-P., Copernicus Publications, State Planet, 2-oae2023, 1, https://doi.org/10.5194/sp-2-oae2023-1-2023, 2023.

Pan, Y., Li, Y., Ma, Q., He, H., Wang, S., Sun, Z., Cai, W.-J., Dong, B., Di, Y., Fu, W., and Chen, C.-T. A.: The role of Mg2+ in inhibiting CaCO3 precipitation from seawater, Mar. Chem., 237, https://doi.org/10.1016/j.marchem.2021.104036, 2021.

Paul, A., Haunost, M., Goldenberg, S., Sanchez Smith, N., and Riebesell, U.: Testing the response of natural plankton community to ocean alkalinity enhancement in the subtropical North Atlantic Ocean, EGU General Assembly 2023, Vienna, Austria, 23–28 Apr 2023, EGU23-9528, https://doi.org/10.5194/egusphere-egu23-9528, 2023.

Perez, F. F. and Fraga, F.: Association constant of fluoride and hydrogen ions in seawater, Mar. Chem., 21, 161–168, https://doi.org/10.1016/0304-4203(87)90036-3, 1987.

Pierrot, D., Lewis, E., and Wallace, D. W. R.: MS Excel Program Developed for CO$_2$ System Calculations, ORNL/CDIAC-105a, Carbon Dioxide Information Analysis Center, Oak Ridge National Laboratory, U.S. Department of Energy [code], Oak Ridge, Tennessee, 2006.

Pytkowicz, R.: Calcium carbonate retention in supersaturated seawater, Am. J. Sci., 273, 515–522, https://doi.org/10.2475/ajs.273.6.515, 1973.

Renforth, P. and Henderson, G.: Assessing ocean alkalinity for carbon sequestration, Rev. Geophys., 55, 636–674, https://doi.org/10.1002/2016rg000533, 2017.

Riebesell, U., Basso, D., Geilert, S., Dale, A. W., and Kreuzburg, M.: Mesocosm experiments in ocean alkalinity enhancement research, in: Guide to Best Practices in Ocean Alkalinity Enhancement Research, edited by: Oschlies, A., Stevenson, A., Bach, L. T., Fennel, K., Rickaby, R. E. M., Satterfield, T., Webb, R., and Gattuso, J.-P., Copernicus Publications, State Planet, 2-oae2023, 6, https://doi.org/10.5194/sp-2-oae2023-6-2023, 2023.

Rogelj, J., Schaeffer, M., Friedlingstein, P., Gillett, N. P., van Vuuren, D. P., Riahi, K., Allen, M., and Knutti, R.: Differences between carbon budget estimates unravelled, Nat. Clim. Change, 6, 245–252, https://doi.org/10.1038/nclimate2868, 2016.

Sánchez, N., Goldenberg, S. U., Brüggemann, D., Weichler, M., Dorssers, S., and Riebesell, U.: Ecosystem impacts of Ocean Alkalization in an oligotrophic marine plankton community: A mesocosm study, EGU General Assembly 2023, Vienna, Austria, 23–28 Apr 2023, EGU23-15436, https://doi.org/10.5194/egusphere-egu23-15436, 2023.

Schuiling, R. D. and Krijgsman, P.: Enhanced Weathering: An Effective and Cheap Tool to Sequester CO$_2$, Climatic Change, 74, 349–354, https://doi.org/10.1007/s10584-005-3485-y, 2006.

Schulz, K. G., Bach, L. T., and Dickson, A. G.: Seawater carbonate chemistry considerations for ocean alkalinity enhancement research: theory, measurements, and calculations, in: Guide to Best Practices in Ocean Alkalinity Enhancement Research, edited by: Oschlies, A., Stevenson, A., Bach, L. T., Fennel, K., Rickaby, R. E. M., Satterfield, T., Webb, R., and Gattuso, J.-P., Copernicus Publications, State Planet, 2-oae2023, 2, https://doi.org/10.5194/sp-2-oae2023-2-2023, 2023.

Sterling, S., Halfyard, E., Hart, K., Trueman, B., Grill, G., and Lehner, B.: Addition of Alkalinity to Rivers: a new CO$_2$ Removal Strategy, ESS Open Archive, https://doi.org/10.22541/essoar.168380809.92137625/v1, 2023.

Suitner, N.: Dataset_Supplement_Suitner_et_al_2024, Zenodo [data set], https://doi.org/10.5281/zenodo.13943981, 2024.

Turek, M. and Gnot, W.: Precipitation of magnesium hydroxide from brine, Ind. Eng. Chem. Res., 34, 244–250, https://doi.org/10.1021/ie00040a025, 1995.

UNFCCC: Report of the Conference of the Parties to the United Nations Framework Convention on Climate Change (21st Session, 2015: Paris), Retrieved December Vol. 4, 2015.

Vassallo, F., La Corte, D., Cancilla, N., Tamburini, A., Bevacqua, M., Cipollina, A., and Micale, G.: A pilot-plant for the selective recovery of magnesium and calcium from waste brines, Desalination, 517, 115231, https://doi.org/10.1016/j.desal.2021.115231, 2021.

Wurgaft, E., Steiner, Z., Luz, B., and Lazar, B.: Evidence for inorganic precipitation of CaCO3 on suspended solids in the open water of the Red Sea, Mar. Chem., 186, 145–155, https://doi.org/10.1016/j.marchem.2016.09.006, 2016.

Wurgaft, E., Wang, Z. A., Churchill, J. H., Dellapenna, T., Song, S., Du, J., Ringham, M. C., Rivlin, T., and Lazar, B.: Particle Triggered Reactions as an Important Mechanism of Alkalinity and Inorganic Carbon Removal in River Plumes, Geophys. Res. Lett., 48, 277, https://doi.org/10.1029/2021gl093178, 2021.

Yang, B., Leonard, J., and Langdon, C.: Seawater alkalinity enhancement with magnesium hydroxide and its implication for carbon dioxide removal, Mar. Chem., 253, 104251, https://doi.org/10.1016/j.marchem.2023.104251, 2023.

Zeebe, R. and Wolf-Gladrow, D.: CO$_2$ in Seawater: Equilibrium, Kinetics, Isotopes, Elsevier Oceanography Book Series, 65, Amsterdam, 361 pp., ISBN 978-0-444-50579-8, 2001.

Zhu, T. and Dittrich, M.: Carbonate Precipitation through Microbial Activities in Natural Environment, and Their Potential in Biotechnology: A Review, Front. Bioeng. Biotechnol., 4, 4, https://doi.org/10.3389/fbioe.2016.00004, 2016.